Journal of Cultural Heritage 53 (2022) 80–87

Contents lists available at ScienceDirect

Journal of Cultural Heritage

journal homepage: www.elsevier.com/locate/culher

Case study

Diagnostic investigation to support the restoration of the polychrome terracotta relief "*Madonna and Child*" in Piove di Sacco (Padova, Italy)

Giovanna Vasco[a], Antonio Serra[a], Daniela Manno[a], Giovanni Buccolieri[a], Lucio Calcagnile[a], Lidiana Miotto[b], Ludovico Valli[c], Alessandro Buccolieri[a,*]

[a] CEDAD (CEnter of Applied Physics, DAting and Diagnostics) - Dipartimento di Matematica e Fisica "Ennio De Giorgi", University of Salento, Lecce, Italy
[b] Centro Restauro Materiale Cartaceo, via R. Caracciolo 6, Lecce, Italy
[c] Dipartimento di Scienze e Tecnologie Biologiche e Ambientali, University of Salento, S.P. 6, Monteroni, Lecce, Italy

ARTICLE INFO

Article history:
Received 10 June 2021
Accepted 23 November 2021

Keywords:
Terracotta relief
Papier-mâché
Polychrome
ED-XRF
Raman
FT-IR
Radiographic investigations

ABSTRACT

Restoration procedures of the polychrome terracotta relief "*Madonna and Child*" with papier-mâché inserts from a shrine in Piove di Sacco (Padova, orthern Italy) were assisted by analytical investigations, contributing to identify the chemical composition of the pigments, fractures and internal damages, additions and retouchings, which strongly modified the original manufact.

In particular, energy dispersive X-ray fluorescence, Raman spectroscopy and FT-IR spectroscopy were employed to determine the chemical composition of pigments on the original layer and on the overpaintings and to understand the artistic techniques. Moreover, X-ray planar radiography and computed tomography were used to understand the structure and its conservative state.

Finally, the relief, stylistically dated to the 17th century, turned out to be a Renaissance terracotta artefact. The polychrome blue traces of lapis lazuli highlighted a valuable artwork and the resemblance with the style of Donatello and his apprentices have recently led to further studies, as an initial part of a larger research on polychrome terracotta in Veneto.

Introduction

The production of polychrome devotional reliefs, well established during the Middle Ages, spread out particularly from Renaissance onward with a serial-production, thanks to an increasing demand for devotional domestic and architectural decorations [1–4]. These gilded and painted artworks, usually representing Madonna and Child, were realized in workshops using moulds from an original model or from direct replicas [5–8].

However, despite the numerous reliefs that are exhibited or preserved in museums, catalogued in private collections or sold on the art market [1–5] with more attention given to glazed artworks [9–11], there are only a few studies on glazed terracotta masterpieces [12–16], and even fewer on those from the Renaissance period [17–20]. According to Brinkmann et al., this is because glazed terracotta objects have long been considered minor artworks. Moreover, the polychrome technique used to decorate these objects has been rejected by many thinkers over the centuries [21]. Consequently, an in-depth study of polychrome terracotta artefacts is necessary, especially during their restoration.

The object of this study, "*Madonna and Child*", is a polychrome terracotta relief with a temple-like shape and a superficial layer of papier-mâché inserts, incorporated into a stone niche placed on the left side of the main entrance of the Immaculate Conception Hospital in Piove di Sacco. Fig. 1 shows the manufact before restoration (Fig. 1a), during the reconstruction with a cellulose fibre-based mixture (Fig. 1b) and after restoration (Fig. 1c).

Its modification by several interventions through times is justified by the devotional value it still has for the townspeople, probably together with the architectural renovations that have led to the displacement of the relief. Indeed, until the 1960s the shrine was in the centre of the hospital entrance, where the *Lazzaretto Vecchio* was during the 17th century plague epidemic. During the last relocation, the work probably fell, since lime and cement used for anchoring the relief to the niche was also used for a hasty intervention to rejoin a deep fracture.

The papier-mâché has drawn attention, considering there are few evidences of this kind of material in the same region, like the important relief of "*Madonna and Child*" of Castelfranco Veneto realized by Jacopo Sansovino [22]. During the removal of the relief, fragments of a stone frame emerged, unfortunately completely

* Corresponding author at: Dipartimento di Matematica e Fisica "Ennio De Giorgi", University of Salento, Lecce, Italy.
E-mail address: alessandro.buccolieri@unisalento.it (A. Buccolieri).

https://doi.org/10.1016/j.culher.2021.11.009
1296-2074/

Fig. 1. Photo of the manufact before restoration (a), during the reconstruction with a cellulose fibre-based mixture (b) and after the restoration (c).

damaged, which is the same of the one on the right side of the Sant'Angelo church in Piove di Sacco.

The terracotta artefact presented vacuoles, lesions, exfoliation, suggesting impure materials rich in metals and baked in a reducing atmosphere, with author's fingerprints and marks left by the straw bed, and a surface covered by papier-mâché inserts, stylistically dated to 17th century, which turned out to be non-original additions during re-painting and/or restoration.

Therefore, in agreement with the Superintendence they were removed, as the repaintings, thus discovering the original terracotta version with polychrome traces, stylistically characterized by classic late Renaissance canons, with elements recalling Francesco II Carrarese, who dominated Piove di Sacco (14th-15th century).

The striking resemblance with the characteristic *stiacciato* technique of Donatello and the artworks of the Madonna of Verona typology, copied by several apprentices, has recently raised interest, leading to more historical research, still in progress, including new projects for the terracotta production in Veneto. Hence, non-invasive and microinvasive investigations were performed on the relief before restoration. Fourier transform infrared spectroscopy and Raman spectroscopy were employed to obtain information on the nature of the support, papier-mâché and polychrome, radiological investigations to examine the artefact internal structure and its conservation state and ED-XRF analysis to identify the characteristic elements of the pigments and decorative elements.

In the cultural heritage field, radiographic techniques are used as they allow to view any structural damage, the presence of nails or bars, any internal structures and to define the artefact conservation state, the historical period and even the authenticity of the studied manufact [23]. In this study, radiographic investigations aimed at assessing the condition, primarily on the boards or slats supporting the work, the cavity inside the cardboard, the fabrication techniques, the surface finish, the presence of fastening systems, their state of preservation and the type of cloth used by the artist.

2. Research aim

Non-invasive and microinvasive diagnostic investigations were performed before and during the restoration work of a polychrome terracotta relief with papier-mâché inserts from a shrine in Piove di Sacco (Padua, Northern Italy). The methodological approach of this archaeometric study exploited X-ray planar radiography and computed tomography to identify fractures and internal damages of the structure and both portable and benchtop energy dispersive X-ray fluorescence, Raman spectroscopy, FT-IR spectroscopy, X-ray diffraction were used to characterize the chemical composition of the pigments both of the original layer and the repainting, which strongly modified the original relief. In fact, the artwork being investigated was stylistically dated to the 17th century, but it turned out to be Renaissance, after the identification and removal of the additions. The polychrome traces of blue of lapis lazuli highlighted a valuable artwork and the resemblance with the style of Donatello and his apprentices have recently led to further studies, as an initial part of a larger research on polychrome Renaissance terracotta reliefs in Veneto. Each point of analyses and the techniques used are listed in Table 1.

3. Material and methods

3.1. Energy dispersive X-ray fluorescence

ED-XRF investigations were carried out prior to the restoration on the surface layer of papier-mâché to characterize its pigments and to identify the period of construction and the presence of subsequent restoration works.

The analysis was performed by using a portable ED-XRF instrument designed at the University of Salento [24,25]. It is composed by an X-ray tube produced by MOXTEK with a Pd-anode operating at 1–40 kV of voltage and 0–100 μA of current. The spectra were registered using a lateral resolution of approximately 1.5 cm^2, 15 kV of voltage, 3 μA of current and an acquisition time of 120 s.

3.2. FT-IR and raman spectroscopy

Infrared analysis was performed by means of a Fourier Transform Infrared (FT-IR) spectrometer Perkin Elmer model Spectrum One. Spectra were collected operating in attenuated total reflection (ATR). Each spectrum is the average of 32 scans (4 cm^{-1} resolution) in the range from 650 to 4000 cm^{-1} using as internal reflection element (IRE) a three-bounce 4 mm diameter diamond microprism (SensIR Technologies, Danbury, CT, USA). Raman scattering measurements were performed by using a MicroRaman spectrometer Horiba model Xplora equipped with 532 nm, 638 nm and 785 nm laser sources and Xplora INV microscope with CCD. For all the samples, the laser source at 532 nm was used and twenty accumulations were acquired for 100 s and repeated on ten different points, thus obtaining an average of spectra.

Owing to the poor preservation state, the paper material consisted of highly displaced worn and weakened fibres, so that analyses were acquired directly on the sampled paper flakes with the visible coloured traces. In fact, cross sections were avoided due to the dislocation and degradation of the fibres that would have been caused overlapping of the signal from the penetration of the polymer.

3.3. Radiographic and computed tomography investigations

The internal structure was investigated by using radiography with General Electric Medical System remote controlled device, obtaining density images based on X-rays which highlight overlapping volumes and different materials. The images were obtained using 120 kV and 60 mA for 30 s.

Computed tomography with the General Electric Medical System multilayer system with spiral technique allowed to elaborate 3D and multiplanar reconstructions. The images were processed with a CR AGFA system.

3.4. XRD analysis

X-ray diffraction analyses were performed by using a diffractometer Rigaku model Mini Flex with Cu-Kα radiation (λ = 0.154 nm). The measurements were carried out with 30 kV accelerating voltage, 15 mA current, scan angle in 2θ from 10° to 80°, with step size of 0.01° and scan speed of 0.05°·s^{-1}. Three scans for each measurement were performed.

Table 1
Pigments analysed with the description of colour, analytical technique used and main result obtained.

Layer	Sample	Colour		Analytical technique	Main result	
1	01	Skin tone (upper layer)		XRF	Fe^{I}, Zn^{II}, Ca^{III}, Ti^{III}, Pb^{III}	
	02	Skin tone (base)			Ti^{I}, Zn^{II}, Pb^{II}, Fe^{III}, Ca^{III}	
	03	Blue			Ti^{I}, Fe^{I}, Zn^{II}, Pb^{II}, Ca^{III}, Cu^{tr}	
	04	Gilding			Cu^{I}, Zn^{II}, Ca^{III}, Fe^{tr}	
	05	Blue			Ti^{I}, Zn^{I}, Pb^{I}, Fe^{II}, Ca^{III}	
	06	Base			Fe^{I}, Zn^{II}, Pb^{II}, Ca^{III}, Ti^{tr}	
	07	Gilding			Cu^{I}, Zn^{II}, Ti^{II}, Pb^{III}	
	08	Base			Pb^{I}, Ca^{II}, Fe^{II}, Zn^{III}, Cu^{tr}	
	09	White			Ca^{I}, Fe^{II}, Zn^{III}, Cu^{III}, Pb^{III}	
	10	Red			Fe^{I}, Ca^{II}, Pb^{II}, Zn^{III}, Cu^{III}	
	11	Red			Pb^{I}, Hg^{II}, Fe^{III}	
	12	Gilding			Cu^{I}, Pb^{II}, Zn^{II}, Fe^{II}, Ca^{III}	
	13	Gilding			Cu^{I}, Zn^{II}, Fe^{III}, Ca^{III}, Ti^{tr}	
	14	Blue			Pb^{I}, Zn^{II}, Ca^{II}, Fe^{II}, Cu^{II}, Ti^{tr}	
	15	Gilding			Cu^{I}, Zn^{II}, Pb^{II}, Ti^{II}, Fe^{III}	
	16	Blue			Pb^{I}, Ti^{II}, Cr^{II}, Zn^{II}, Fe^{II}, Cu^{III}, Ca^{III}	
	17	Red			Hg^{I}, Pb^{I}, Cu^{II}, Zn^{III}, Fe^{tr}, Cr^{tr}, Ti^{tr}	
	18	Child's cheek	Base	FT-IR	3546, 3400, 1077 cm^{-1} (S–O)	Gypsum
					1410, 875 cm^{-1} (CO_3^{2-})	Carbonate
					1640, 1618 cm^{-1} (OH)	Binder and paper
					1725 cm^{-1} (C = O)	
					2920, 2851 cm^{-1} (CH_2)	
			Blue	Raman	336, 452, 990, 1148 cm^{-1}	Lithopone
	19	Child's head Base		FT-IR	1019 cm^{-1} (S–O)	Gypsum
					1416–873 cm^{-1} (CO_3^{2-})	Carbonate
					2920, 2851 cm^{-1} (CH_2)	Binder and paper
					3525, 1640 cm^{-1} (OH)	
					1734 (C = O)	
	20	Capital	Base	FT-IR	3524, 3393, 1100, 900 cm^{-1} (S–O)	Gypsum
					1416, 863 cm^{-1} (CO_3^{2-})	Carbonate
					1740 cm^{-1} (C = O)	Binder and paper
					2915, 2840 cm^{-1} (CH_2)	
				Raman	215, 339, 452, 984, 1149 cm^{-1}	Lithopone
			Green	FT-IR	3370 cm^{-1} (OH)	Binder and paper
					2925–2850 cm^{-1} (CH_2)	
					1730 cm^{-1} (C = O)	
					1405, 862 cm^{-1} (CO_3^{2-})	Carbonate
				Raman	338, 359, 375, 405, 449, 830, 978 cm^{-1}	Lead chromate
					254, 273, 344, 418, 446, 478, 603, 978, 988, 1076, 1145, 1177 cm^{-1}	Copper sulphate
			Red	FT-IR	1112, 1045, 1066, 680 cm^{-1}	White lead
					1306, 869 cm^{-1} (CO_3^{2-})	Carbonate
					3370 cm^{-1} (OH)	Binder and paper
					2925, 2850 cm^{-1} (CH_2)	
					1306, 869 cm^{-1} (CO_3^{2-})	
					1730 cm^{-1} (C = O)	
				Raman	212, 239, 277, 320 cm^{-1}	Vermilion or Cinnabar
	21	Frame		Raman	237, 269, 328 cm^{-1}	Vermilion or Cinnabar
	22	Floral garlands		FT-IR	3523, 3396, 1052 cm^{-1} (S–O)	Gypsum
					1404, 873 cm^{-1} (CO_3^{2-})	Carbonate
					2926, 2848 cm^{-1} (CH_2)	Binder and paper
				Raman	288, 539, 581, 808, 1096, 1357 cm^{-1}	Lazurite
	23	Child's foot		FT-IR	3522, 3394, 1052 cm^{-1} (S–O)	Gypsum
					2926, 2848 cm^{-1} (CH_2)	Binder and paper
					1404, 874 cm^{-1} (CO_3^{2-})	Carbonate
	24	Background next to the Child		Raman	268, 272, 548, 806, 808, 1096, 1346 cm^{-1}	Lazurite
	25	Virgin's cheek		FT-IR	1744 cm^{-1} (C = O)	Binder and paper
					1640, 1618, 1406 cm^{-1} (OH)	
					2926, 2848 cm^{-1} (CH_2)	
					1404, 876 cm^{-1} (CO_3^{2-})	Carbonate
					3534, 3393, 1080 cm^{-1} (S–O)	Gypsum
	26	Floral garlands	Base	FT-IR	1640, 1618 cm^{-1} (OH)	Binder and paper
					2915, 2847 cm^{-1} (CH_2)	
					1405, 873 cm^{-1} (CO_3^{2-})	Carbonate
					3544, 3404, 1071 cm^{-1} (S–O)	Gypsum
			Green	Raman	351, 832 cm^{-1}	Lead chromate
			Blue		243, 298, 549, 578, 808, 1096, 1352 cm^{-1}	Lazurite
			Red		255, 287, 346 cm^{-1}	Vermilion or Cinnabar

(*continued on next page*)

Table 1 (*continued*)

Layer	Sample	Colour		Analytical technique	Main result	
	27	Virgin's mantle		Raman	258, 282, 543, 580, 804, 1096, 1360 cm^{-1}	Lazurite
	28	Background	Base	FT-IR	820 cm^{-1} ($PbCrO_4$)	Lead chromate
					2940, 2847, 1633, 1618 cm^{-1} (OH)	Binder and paper
					1732, 862 cm^{-1} (C = O)	
					1415 cm^{-1} (CO_3^{2-})	Carbonate
			Blue	Raman	260, 282, 542, 582 cm^{-1}	Lazurite
			Yellow		256, 284, 359, 405, 844, 975 cm^{-1}	Lead chromate
	29	Brown		FT-IR	1641, 1618 cm^{-1} (OH)	Binder and paper
					1744 cm^{-1} (C = O)	
					2923 cm^{-1} (CH_2)	
					1414, 872 cm^{-1} (CO_3^{2-})	Carbonate
					3546, 3420, 1049 cm^{-1} (S–O)	Gypsum
	30	Virgin's mantle	Base	FT-IR	1640, 1618 cm^{-1} (OH)	Binder and paper
					1724 cm^{-1} (C = O)	
					2927, 2839 cm^{-1} (CH_2)	
					1419, 874 cm^{-1} (CO_3^{2-})	Carbonate
					3525, 3416, 1059 cm^{-1} (S–O)	Gypsum
			Blue	Raman	235, 254, 597, 682, 749, 956, 1037, 1145, 1341, 1456, 1532, 1597 cm^{-1}	Phtalocyanine blue
			Red		256, 289, 346, 412 cm^{-1}	Vermilion or Cinnabar
2	31	Blue		Raman	260, 547, 585, 808, 1092 cm^{-1}	Lazurite
					1364, 1637 cm^{-1}	Carbon black
	32	Blue and black		Raman	259, 549, 585, 810, 1092 cm^{-1}	Lazurite
					1372, 1594 cm^{-1}	Carbon black
					141, 283, 387, 947 cm^{-1}	Blixite
	33	Red		Raman	139, 362, 380, 843 cm^{-1}	Crocoite
					258, 549, 588, 805, 1096 cm^{-1}	Lazurite
					211, 256, 286, 347 cm^{-1}	Vermilion or Cinnabar
					1357, 1637 cm^{-1}	Carbon black
	34	Green		Raman	256, 547, 585, 800, 1091 cm^{-1}	Lazurite
					1357, 1646 cm^{-1}	Carbon black
	35	Black		Raman	1354 1596 cm^{-1}	Carbon black
	36	Green		Raman	141, 339, 359, 380, 407, 840 cm^{-1}	Crocoite
					233, 438, 612, 785 cm^{-1}	Rutile
					1352, 1600 cm^{-1}	Carbon black
	37	Red		Raman	162, 225, 311, 387, 481, 549, 623, 709, 871, 1086 cm^{-1}	Minium
	38	Blue		Raman	147, 195, 398, 519, 643 cm^{-1}	Anatase
					256, 547, 586, 806, 1096 cm^{-1}	Lazurite
					1357, 1642 cm^{-1}	Carbon black
	39	Brown		Raman	262, 545, 586, 808, 1094 cm^{-1}	Lazurite
					136, 364, 380, 841 cm^{-1}	Crocoite
					1366, 1642 cm^{-1}	Carbon black

I: main element; II: secondary element; III: minority element; tr: trace element.

4. Results and discussion

4.1. Structure

The axial sections examination shows parallelepiped-shaped support whose thickness varies from 28 to 33 mm for the upper 2/3, up to 40 mm in the lower sector, with a wide-ranging front concavity of about 350–400 UH (Hounsfield Unit), while the superposed overhang with the Madonna and Child has an average density of 600–700 UH. The artwork is presumably realized in single heat treatment, considering there is no interruption between the support and the overhang.

Throughout selective scans on the projection in the lower median section on the frame, different material composition is detected compared to the support, which has a lower density (130–190 UH).

The frame is mostly coated with a fragmented hyperdense foil on its surface, with a high density greater than 3700 UH, due to a metal used for a gilding decoration (corresponding to the areas with copper identified by using ED-XRF). At the same level, in the support thickness, there is a spherical formation (15 mm) with metallic density and a hypodense nucleus connected to the surface.

The 3D reconstruction with separation of densities allows to highlight in white the residues of the metal foil, particularly abundant on the back of the Child and the upper external sectors, on the support with an arborescent aspect. Planar reconstructions, parallel to the support, highlight a traumatic fracture from the upper left external corner of the support, with an oblique profile and a triangular gap, stuffed by a filling in which there is a hyperdense metal fragment.

The body of the work is apparently made up of multiple and coarse fragments with distinct margins, separated by empty space, due to fractures during the heat treatment phase, which appear to be gypsumed on the surface.

The radiological investigation shows manual processing obtained with various jointed and consolidated terracotta masses heated in a single firing. Fig. 2 shows a radiography of the studied artefact, which highlights one of the two nails of the relief.

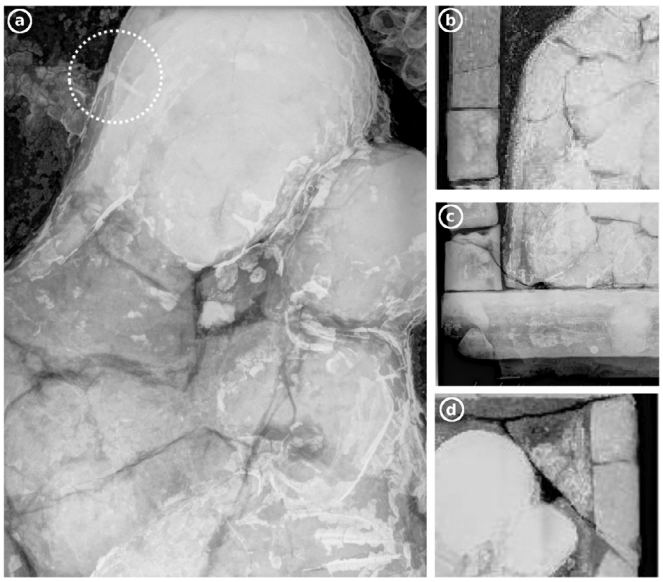

Fig. 2. Radiography of the studied artefact. The dotted circle in (a) highlights one of the two nails of the relief, while the fractures of the frame are shows in (b-d).

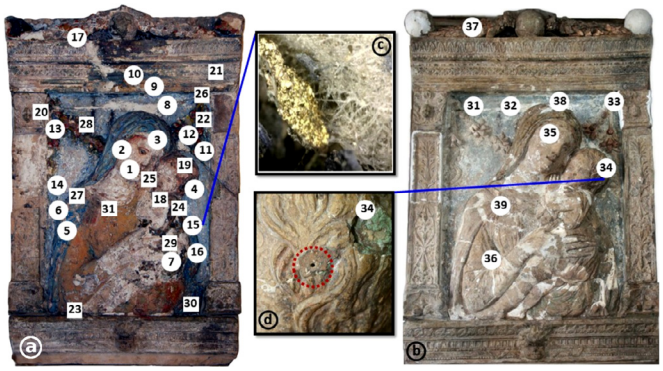

Fig. 3. Photo of the terracotta relief before the restoration work with the measuring points of the areas investigated via portable ED-XRF (circles) and of the areas sampled for Raman and FT-IR spectroscopy (squares) (a). Photo of the sampling areas after the removal of the papier-mâché inserts (b). Optical microscope image (at 100 x) of cellulose fibres and gilding traces in the sample n. 15 (c). Green stucco and vent hole in the sample n. 34 (d).

4.2. Pigments

Fig. 3a shows the terracotta relief before restoration with the measuring points of investigated areas by using portable ED-XRF and those sampled for Raman and FT-IR spectroscopy. Fig. 3b shows the sampling areas after the papier-mâché removal. The main experimental results are summarized in table 1, which divides the 39 point of analysis (n. 1–17 non invasive analyses, n. 18–39 sampled fragments) into two layers. Layer 1 (samples n. 1–30), the upper layer, refers to the papier-mâché layer which was on the terracotta relief before restoration, while layer 2 (samples n. 31–39), the underlying layer, refers to that analysed subsequently the papier-mâché removal and located directly on the terracotta. It must point out that between the non-invasive analyses and the sampling phase a first cleaning was performed by conservators. For each sample, the colour, the analytical technique and the main result obtained are reported.

The results obtained for the pigments by using the above-mentioned techniques of investigation are consistent with each other. Indeed, in most of the measuring points taken for the ED-XRF, used as a preliminary and non-invasive method, several elements belonging to different colours were detected, highlighting a sequence of numerous re-paintings, which were further investigated after collecting some samples analysed via Raman and FT-IR spectroscopy.

Regarding the upper layer, the detection of hydrocerussite ($Pb_3(CO_3)_2(OH)_2$) for sample n. 20 and the widespread presence of lead indicate the use of white lead [$(PbCO_3)_2 \bullet Pb(OH)_2$], probably employed both as primer and white pigment. About the chemical groups detected via FT-IR spectroscopy, the carbonate group can be associated both to white lead and calcium carbonate, since calcium was extensively found on the whole surface. However, the abundant presence of sulphates implies the use of gypsum for the ground layer of the paper additions, used with white lead and calcium carbonate, except for the samples n. 22, n. 23, n. 25 and n. 29 where gypsum was determined as matrix of the pigment. Regarding the binder, it was not possible to definitively determine its animal or vegetal nature because the eventual proteinaceous, glycoside or lipid components were covered by the abundant detection of the preparation materials. In fact, despite the carbonyl group probably belongs the binder, methyl and hydroxyl groups are linked to cellulose, the main constituent of papier-mâché. Moreover, the presence of gypsum did not allow to discriminate the possible animal origin based on the sulphate bond, while no disulphide bridge was detected. Fig. S1 shows the FT-IR spectrum of sample n. 18. Zinc and titanium may be associated to non-original white pigments used in different interventions on the artworks, that could be re-painting and/or restoration. The former, despite being known since antiquity, was not used as a pigment until the end of the 18th century to replace the toxic white lead, being industrially improved around the middle of the 19th century [26,27]. The industrialization of the second (TiO_2) began instead between 1910 and 1920 CE [28]. Via Raman spectroscopy, lithopone ($BaSO_4 \cdot ZnS$), a white pigment discovered in the 1870s and manufactured from the late 19th century, was detected on some paper insertions (samples n. 18, n. 20).

The skin tone was created combining white colours with a red pigment based on iron oxide, extensively found for the red hues on all the relief, which is the main component of ochres and compounds with tones from yellowish to brownish shades [29]. However, vermilion or cinnabar (if referred to the mineral) [30,31], was detected in some areas both by X-ray fluorescence (point n. 11, n. 17) and Raman spectroscopy (sample n. 20, n. 21, n. 26, n. 30). Fig. S2 shows Raman spectrum of sample n. 26.

Regarding the blue pigments, the elements revealed during the non-invasive measurements were iron, usually related to Prussian blue ($C_{18}Fe_7N_{18}$), and copper to a small extent, connected both to azurite ($Cu_3(CO_3)_2(OH)_2$) and phthalocyanine blue ($C_{32}H_{16}CuN_{18}$) [32]. In particular, high copper in point n. 14 suggests the use of azurite. However, exact reconstruction of blue is not possible, even considering the various layers determined for the pigments listed in Table 1.

Thanks to Raman spectroscopy, in most of blue samples (n. 22, n. 24, n. 26, n. 28, n. 29) lazurite was detected, a cubic sodic-calcic aluminosilicate sulphate mineral [$(Na,Ca)_8[(Al,Si)_{12}O_{24}](S,SO_4)$], member of feldspathoid and sodalite groups with a blue hue given by the presence of S^{3-}, usually mined in Afghanistan [33].

Furthermore, sample n. 30 turned out to be phthalocyanine blue, a modern synthetic organic pigment used from the 20th century, belonging to a large group of synthetic organic macromolecules, which consists of macrocyclic ligand complexes with copper as principal metal ion chelated and chlorine and bromine as peripheral substituents.

However, Prussian blue and azurite were not determined by Raman spectroscopy, despite reasonably supposed by EDXRF, since they were considered fairly localized integrations, then removed during the cleaning treatment.

Considering the green layers, a combination of copper sulphate and lead chromate was identified in sample n. 20. Given that this green mixture should be realized with blue and yellow pigments, copper sulphate has to be in the most common pentahydrate form, which is blue, while lead chromate, used since the first quarter of the 19th century, has a colour range from yellow to red, because of the variable surrounding which causes changes in the crystal structure [34,35]. This compound agrees with the elements detected in point n. 16. Lead chromate was also identified in samples n. 26 and 28 with the presence of lazurite. Fig. S3 shows FT-IR spectrum of sample n. 28.

In points n. 4, n. 7, n. 12, n. 13, n. 15, characterized by the detachment of the more superficial pictorial layers, a considerable amount of copper was found, propably used for an imitation of gilding [36,37].

Fig. 3c shows an optical microscope image of point n. 15, highlighting the cellulose fibres and gilding traces.

After removing the paper inserts, samples of several pigmented traces of an older layer were investigated via Raman spectroscopy. Sample n. 31 presents the Raman spectrum of amorphous carbon, which is characterized by broad bands around 1350 cm^{-1} and 1640 cm^{-1} with large variability in the actual positions of these two signals, depending on the hybridization and the allotropic form based on the firing temperature [38]. Their production starts with the incomplete combustion of carbon-rich organic materials so that the spectrum profile is very similar for black pigments obtained from different substances. Moreover, it was noticed carbon black is distributed above all in combination with lazurite for blue samples, presumably to darken the shade. However, considering its spread, it cannot be excluded as an external contaminant due to candles usually placed in front of devotional artworks.

Lazurite, related to blue of lapis lazuli, was abundantly detected in samples n. 31, n. 32 and n. 38. However, also in samples n. 33, n. 39 and n. 34 were identified few small traces of lazurite [39,40].

Considering the last one (sample n. 34) had a green shade and was employed as stucco. Fig. 3d shows a green stucco and vent hole in the sample n. 34.

Green fragments (n. 34, n. 36) were sampled respectively from a cavity located on the Child's head and from a gap in the Virgin's arm, therefore assumed to be a filler. Since no Raman scattering was detected via Raman spectroscopy, X-ray diffraction analysis was then performed on sample n. 34, highlighting the presence of calcite bounded with other materials that were not identified. The same sample was analysed via micro-X-ray fluorescence, revealing barium, calcium, iron and a significant amount of lead. Therefore, the analysed material was a stucco admixed with white pigments including white lead, calcium carbonate and carbonate or barium sulfate. Sulfur signal (2.2 keV) can only be hypothesized as it is masked by line M of lead, but it is reasonable since baryte has a greyish-greenish colour as the sample. Iron can refer both to contaminations occurred during the production processes of lead carbonate and to impurities in baryte, which may have given the reddish colour to some grains of the sample. Depending on the purity of white lead, the presence of other substances and the procedures adopted in certain geographical areas, white pigments took different names. In the 19th century, Venice white was produced, consisting of lead carbonate and barium sulphate with the presence of iron as a contaminant, especially if baryte was imported from Austria, so the result was an alteration of the original white colour. Moreover, this material can agree with the artwork location. The production methods and the problems deriving from impurities and contaminants for the creation of white pigments containing lead are described in detail in the *New universal Technological or Arts and Crafts Dictionary*, published for the first time in Italy in the 1930s in Venice. Baryte and white lead allows to date the period of probable application of this stucco between the 19th and first half of the 20th century. Indeed, at the end of the 18th century, due to the toxicity of white lead, several attempts were made to produce other types of white pigments. The use of barium white became frequent from the early decades of the 19th century, while white lead was banned in several countries from 19 November 1921 CE due to the International Labour Organization through the stipulation of an agreement, signed by Italy in 1952 CE.

Regarding red pigments, sample n. 37, taken from the decorative red leaf in the background, is based on minium, a mixed lead oxide containing Pb^{2+} and Pb^{4+} ions used as a pigment since antiquity, while sample n. 33 has vermilion or cinnabar (HgS). Nonetheless, traces of crocoite ($PbCrO_4$) were identified, rarely used in the past and usually related to a contemporary pigment made from an orange-red lead chromate mineral first found in 1770 CE in Ekaterinburg, Russia [41–43]. The same was detected in samples n. 39 and n. 36, where rutile was found, indicating titanium white. Other traces of inauthentic pigment employed during restorations were detected in sample n. 32 with blixite ($Pb_8O_5(OH)_2Cl_4$), a pale-yellow mineral discovered in 1958 CE [35,44], and in sample n. 38 with anatase, the other allotropic form of titanium oxide. Fig. S4 shows Raman spectrum of sample n. 38 (Fig. 4).

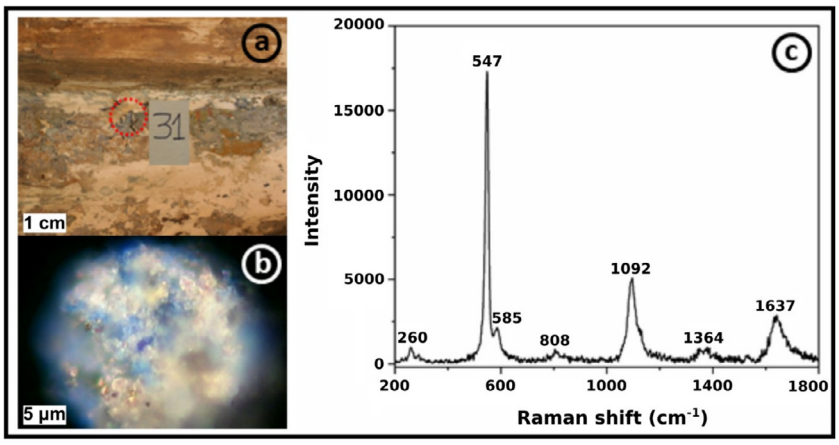

Fig. 4. Photo of the sampling areas of the sample n. 31 (a), optical microscope image at 50 x (b) and Raman spectrum (c).

5. Conclusion

Diagnostic investigations supported the step-by-step restoration of a terracotta relief covered by a layer of papier-mâché. Radiological studies provided information on the terracotta processing, the presence of important fractures and traces of metal foils. The latter, on the basis of the analysis carried out using portable EDXRF, were found to be made of copper. It was supposed that such metal foils were used in the realisation of the terracotta work to imitate the gilding process.

The FT-IR and Raman spectroscopies allowed to identify that the artwork had undergone several repaintings in the course of different restorations that changed its appearance several times over time.

For example, the surface layer of papier-mâché turned out to be a later addition that was hiding the original glazed Renaissance terracotta surface.

Only a few fragments remained of the original polychrome decoration, which were analysed in this paper. In particular, the spectroscopic characterisation of these polychrome remains revealed the presence of different pigments such as lapis lazuli blue on the background and red minium and vermilion on the crowns. This information was then used by the conservators to proceed with the painting restoration.

Funding

This research did not receive any specific grant from funding agencies in the public, commercial, or not-for-profit sectors.

Acknowledgments

The authors thank the doctor P. Quarta Colosso for letting us use his equipment in the Radiological Study *Gennaro Quarta Colosso* (Lecce, Italy) and Comieco (National Consortium for Recovery and Recycling of Cellulose-based Packaging) which sponsored the restoration work made by L. Miotto, D. Guida, G. Vasco, I. Memmi, M. Ciardo, M. Palma, E. Coppolella by using Paper Factor, a recyclable and reversible compound based on cellulose fibres by arch. R. Cavaciocchi and L. Miotto. The authors thank the Superintendency for the Historical, Artistic and Ethno-anthropological Heritage for the provinces of Venice, Belluno, Padua and Trevisofor its collaboration. Moreover, the authors thank Massimo Luggeri of the University of Salento, who has contributed to improving the quality of the figures.

Supplementary materials

Supplementary material associated with this article can be found, in the online version, at doi:10.1016/j.culher.2021.11.009.

References

[1] G. Gariani, P. Lehuédé, L. Leroux, G. Wallez, F. Goubard, A. Bouquillon, M. Bormand, First insights on the mineral composition of “stucco” devotional reliefs from Italian Renaissance Masters: investigating technological practices and raw material sourcing, J Cult Herit 34 (2018) 23–32, doi:10.1016/j.culher.2018.05.003.
[2] B. Paolozzi Strozzi, M. Bormand, The Springtime of the Renaissance: Sculpture and the Arts in Florence 1400-60, Mandragora, Florence, 2013.
[3] A.L. Palmer, The Walters’ “Madonna and Child” Plaquette and Private Devotional Art in Early Renaissance Italy, J Walters Art Museum 59 (2001) 73–84.
[4] G.A. Johnson, Art or Artefact ? Madonna and Child Reliefs in the Early Renaissance, in: The Sculpted Object, 1400-1700, Scolar Press, Aldershot, 1997, pp. 1–17.
[5] J. Pope-Hennessy, The interaction of painting and sculpture in Florence in the fifteenth century, J R Soc Arts 117 (1969) 406–424.
[6] G. Gentilini, Sculptura dipinta o pittura a rilievo ?, Riflessioni sulla policromia nel Quattrocento fiorentino, in: M. Bormand, A. Bouquillon (Eds.), Terres Cuites de La Renaissance, Matière et Couleur, Lavandiere, Marie, Paris, 2012.
[7] E. Marchand, Reproducing relief: the use and status of plaster casts in the Italian renaissance, in: Depth of Field: Relief Sculpture in Renaissance Italy, Peter Lang, Oxford, 2007, pp. 191–223.
[8] A. Zucchiatti, A. Bouquillon, B. Moignard, J. Salomon, J.R. Gaborit, Study of Italian Renaissance sculptures using an external beam nuclear microprobe, in: Nuclear Instruments and Methods in Physics Research Section B: Beam Interactions With Materials and Atoms, 161–163, 2000, pp. 699–703, doi:10.1016/S0168-583X(99)00905-2.
[9] M. Sendova, B. Kaiser, M. Scalera, V. Zhelyaskov, Della Robbia blue glaze: micro-Raman temperature study and X-ray fluorescence spectroscopy characterization, J. Raman Spectrosc. 4 (2009) 469–472, doi:10.1002/jrs.2459.
[10] M.I. Dias, M.I. Prudêncio, Z. Kasztovszky, B. Maróti, I. Harsányi, P. Flor, Nuclear techniques applied to provenance and technological studies of Renaissance majolica roundels from Portuguese museums attributed to della Robbia Italian workshop, J Radioanal Nucl Chem 312 (2017) 205–219, doi:10.1007/s10967-017-5235-9.
[11] P. Maravelaki-Kalaitzaki, N. Kallithrakas-Kontos, Pigment and terracotta analyses of Hellenistic figurines in Crete, Anal. Chim. Acta 497 (2003) 209–225, doi:10.1016/j.aca.2003.08.035.
[12] I. Bonaduce, C. Blaensdorf, P. Dietemann, M.P. Colombini, The binding media of the polychromy of Qin Shihuang’s Terracotta Army, J Cult Herit 9 (2008) 103–108, doi:10.1016/j.culher.2007.08.002.
[13] H. Brecoulaki, Precious colours? in Ancient Greek polychromy and painting : material aspects and symbolic values, Revue Archéologique 57 (2014) 3–3, doi:10.3917/arch.141.0003.
[14] J.L. Pérez-Rodrıǵuez, C. Maqueda, M.C. Jiménez de Haro, P. Rodrıǵuez-Rubio, Effect of pollution on polychromed ceramic statues, Atmos. Environ. 32 (1998) 993–998, doi:10.1016/S1352-2310(97)00337-3.
[15] A. Duran, J.L. Perez-Rodriguez, M.C. Jimenez de Haro, Study of the gilding technique used in polychromed stones and ceramics by dedicated laboratory-made micro X-ray diffraction and complementary techniques, Anal Bioanal Chem 394 (2009) 1671–1677, doi:10.1007/s00216-009-2836-3.
[16] C. Colombo, F. Bevilacqua, L. Brambilla, C. Conti, M. Realini, J. Striova, G. Zerbi, Terracotta polychrome sculptures examined before and after their conservation work: contributions from non-invasive in situ analytical techniques, Anal Bioanal Chem 401 (2011) 757–765, doi:10.1007/s00216-011-5085-1.
[17] A. Kriznar, M.V. Muñoz, F. de la Paz, M.A. Respaldiza, M. Vega, Pigment identification using x-ray fluorescence in a polychromated sculpture by Pedro Millán, X-Ray Spectrometry 37 (2008) 355–359, doi:10.1002/xrs.1020.
[18] A. Križnar, M.V. Muñoz, F. de la Paz, M.A. Respaldiza, M. Vega, XRF analysis of two terracotta polychrome sculptures by Pietro Torrigiano, X-Ray Spectrometry 38 (2009) 169–174, doi:10.1002/xrs.1135.
[19] A. Bezur, G. Kavich, J. Stenger, E. Torok, C. Snow, Discovery of challacolloite, an uncommon chloride, on a fifteenth-century polychrome terracotta relief by Michele da Firenze, Applied Physics A 121 (2015) 83–93, doi:10.1007/s00339-015-9386-7.
[20] C. Pelosi, D. Fodaro, L. Sforzini, C. Falcucci, P. Baraldi, The terracotta modelli of Palazzo Venezia in Rome: investigation of the constituent materials for fundamental knowledge and to aid conservation decisions, Studies in Conservation 62 (2017) 266–282, doi:10.1179/2047058415Y.0000000021.
[21] V. Brinkmann, J. Ostergaard, M. Collareta, A. Potts, R. Panzanelli, The Color of life: polychromy in sculpture from antiquity to the present, Los Angeles, 2008. https://books.google.com/books?hl=it&lr=&id=2gQesgryr8oC&oi=fnd&pg=PR8&dq=V.+Brinkmann,+J.+Stubbe+Ostergaard,+M.+Collareta,+A.+Potts,+R.+Pazanelli,+The+color+of+life:+polychromy+in+sculpture+from+antiquity+to+the+present,+J.+Paul+Getty+Museum+Pubns,+Los+A.
[22] A. Buccolieri, G. Buccolieri, A. Castellano, P.Q. Colosso, L. Miotto, Non-destructive techniques used during the restoration of the relief “Madonna and Child” by Jacopo Sansovino, Applied Physics A 120 (2015) 447–453, doi:10.1007/s00339-015-9226-9.
[23] C. Calza, D.F. Oliveira, R.P. Freitas, H.S. Rocha, J.R. Nascimento, R.T. Lopes, Analysis of sculptures using XRF and X-ray radiography, Radiation Physics and Chemistry. 116 (2015) 326–331. https://doi.org/10.1016/j.radphyschem.2015.04.012.
[24] A. Buccolieri, E. Degl’Innocenti, R. Cesareo, A. Castellano, G. Buccolieri, Non-invasive in-situ analysis of a wreath of gold leaves from the National Archaeological Museum of Taranto, Measurement: Journal of the International Measurement Confederation 126 (2018) 164–167, doi:10.1016/j.measurement.2018.05.063.
[25] A. Buccolieri, A. Castellano, E. Degl’Innocenti, R. Cesareo, R. Casciaro, G. Buccolieri, EDXRF analysis of gold jewelry from the Archaeological Museum of Taranto, Italy: EDXRF analysis of gold jewelry, X-Ray Spectrom 46 (2017) 421–426, doi:10.1002/xrs.2761.
[26] H. Kühn, Die Pigmente in Den Gemälden der Schack-Galerie, Munich, 1969.
[27] N. Eastaugh, V. Walsh, T. Chaplin, R. Siddal, Pigment Compendium: A Dictionary of Historical Pigments, Routledge, 2007, doi:10.4324/9780080473765.
[28] B.A. van Driel, K.J. van den Berg, J. Gerretzen, J. Dik, The white of the 20th century: an explorative survey into Dutch modern art collections, Heritage Science 6 (2018) 16, doi:10.1186/s40494-018-0183-4.
[29] F. Froment, A. Tournié, P. Colomban, Raman identification of natural red to yellow pigments: ochre and iron-containing ores, Journal of Raman Spectroscopy 39 (2008) 560–568, doi:10.1002/jrs.1858.
[30] R.J. Gettens, R.L. Feller, in: Vermilion and Cinnabar, in: Artists’ Pigments: A Handbook of Their History and Characteristics, Ashok Roy, Washington D.C., 1999, pp. 159–182.

[31] M. Spring, R. Grout, The Blackening of Vermilion: An Analytical Study of the Process, Paintings, London, 2002.
[32] C. Defeyt, D. Strivay, PB15 as 20th and 21st Artists' Pigments: conservation Concerns, E-Preservation Science 11 (2014) 6–14.
[33] G. Vasco, A. Serra, D. Manno, G. Buccolieri, L. Calcagnile, A. Buccolieri, Investigations of byzantine wall paintings in the abbey of Santa Maria di Cerrate (Italy) in view of their restoration, Spectrochimica Acta - Part A: Molecular and Biomolecular Spectroscopy 239 (2020) 118557, doi:10.1016/j.saa.2020.118557.
[34] V. Otero, L. Carlyle, M. Vilarigues, M.J. Melo, Chrome yellow in nineteenth century art: historic reconstructions of an artists' pigment, RSC Adv 2 (2012) 1798–1805, doi:10.1039/C1RA00614B.
[35] N. Eastaugh, V. Walsh, T. Chaplin, R. Siddall, Pigment Compendium: Optical Microscopy of Historical Pigments, 2nd ed., Routledge, Oxford, 2013, doi:10.4324/9780080454573.
[36] C. Cession, in: The Surface Layers of Baroque gildings: Examination, 35, conservation, restoration, Studies in Conservation, 1990, pp. 33–35, doi:10.1179/sic.1990.35.s1.008.
[37] I. Crina Anca Sandu, M.H. de Sá, M.C. Pereira, Ancient 'gilded' art objects from European cultural heritage: a review on different scales of characterization, Surf. Interface Anal. 43 (2011) 1134–1151, doi:10.1002/sia.3740.
[38] D.B. Schüpfer, F. Badaczewski, J. Peilstöcker, J.M. Guerra-Castro, H. Shim, S. Firoozabadi, A. Beyer, K. Volz, V. Presser, C. Heiliger, B. Smarsly, P.J. Klar, Monitoring the thermally induced transition from sp^3-hybridized into sp^2-hybridized carbons, Carbon N Y 172 (2021) 214–227, doi:10.1016/j.carbon.2020.09.063.
[39] S.A.T. Redfern, Manual of mineralogy, 20th ed., New York, NY, 1995. https://doi.org/10.1002/gj.3350300114.
[40] K. Hettmann, T. Wenzel, M. Marks, G. Markl, The sulfur speciation in S-bearing minerals: new constraints by a combination of electron microprobe analysis and DFT calculations with special reference to sodalite-group minerals, American Mineralogist 97 (2012) 1653–1661, doi:10.2138/am.2012.4031.
[41] D. Hradil, J. Hradilová, P. Bezdička, S. Švarcová, Z. Čermáková, V. Košařová, I. Němec, Crocoite PbCrO4 and mimetite Pb5(AsO4)3Cl: rare minerals in highly degraded mediaeval murals in Northern Bohemia, Journal of Raman Spectroscopy 45 (2014) 848–858, doi:10.1002/jrs.4556.
[42] H. Kühn, M. Curran, Chrome yellow and other chromate pigments, in: Artists' Pigments: A Handbook of Their History and Characteristics, 1986: pp. 187–217.
[43] L. Monico, G. Van der Snickt, K. Janssens, W. De Nolf, C. Miliani, J. Verbeeck, H. Tian, H. Tan, J. Dik, M. Radepont, M. Cotte, Degradation Process of Lead Chromate in Paintings by Vincent van Gogh Studied by Means of Synchrotron X-ray Spectromicroscopy and Related Methods. 1. Artificially Aged Model Samples, Anal. Chem. 83 (2011) 1214–1223, doi:10.1021/ac102424h.
[44] V. Gonzalez, G. Wallez, T. Calligaro, D. Gourier, M. Menu, Synthesizing lead white pigments by lead corrosion: new insights into the ancient manufacturing processes, Corros Sci 146 (2019) 10–17, doi:10.1016/j.corsci.2018.10.033.